Southern Annular Mode drives multicentury wildfire activity in southern South America

Andrés Holz[a,1], Juan Paritsis[b], Ignacio A. Mundo[c,d], Thomas T. Veblen[e], Thomas Kitzberger[b], Grant J. Williamson[f], Ezequiel Aráoz[g], Carlos Bustos-Schindler[h], Mauro E. González[h,i], H. Ricardo Grau[g,j], and Juan M. Quezada[k]

[a]Department of Geography, Portland State University, Portland, OR 97207; [b]Laboratorio Ecotono, Instituto de Investigaciones en Biodiversidad y Medioambiente, Consejo Nacional de Investigaciones Científicas y Técnicas, Universidad Nacional del Comahue, 8400 Bariloche, Argentina; [c]Laboratorio de Dendrocronología e Historia Ambiental, Instituto Argentino de Nivología, Glaciología y Ciencias Ambientales, El Centro Científico Tecnológico, Consejo Nacional de Investigaciones Científicas y Técnicas, M5502IRA Mendoza, Argentina; [d]Facultad de Ciencias Exactas y Naturales, Universidad Nacional de Cuyo, M5502JMA Mendoza, Argentina; [e]Department of Geography, University of Colorado, Boulder, CO 80309; [f]School of Biological Sciences, University of Tasmania, Hobart, TAS 7001, Australia; [g]Instituto de Ecología Regional, Consejo Nacional de Investigaciones Científicas y Técnicas, Universidad Nacional de Tucumán, 4172 Yerba Buena, Argentina Argentina; [h]Instituto de Conservación, Biodiversidad y Territorio, Facultad de Ciencias Forestales y Recursos Naturales, Instituto de Silvicultura, Universidad Austral de Chile, Valdivia, Chile; [i]Center for Climate and Resilience Research (CR2), Santiago, Chile; [j]Facultad de Ciencias Naturales e Instituto Miguel Lillo, Universidad Nacional de Tucumán, 4000 San Miguel de Tucumán, Argentina; and [k]Facultad de Ciencias Forestales, Universidad Nacional de Misiones, Eldorado, 3380 Misiones, Argentina

Edited by Glen M. MacDonald, University of California, Los Angeles, CA, and approved July 24, 2017 (received for review April 1, 2017)

The Southern Annular Mode (SAM) is the main driver of climate variability at mid to high latitudes in the Southern Hemisphere, affecting wildfire activity, which in turn pollutes the air and contributes to human health problems and mortality, and potentially provides strong feedback to the climate system through emissions and land cover changes. Here we report the largest Southern Hemisphere network of annually resolved tree ring fire histories, consisting of 1,767 fire-scarred trees from 97 sites (from 22 °S to 54 °S) in southern South America (SAS), to quantify the coupling of SAM and regional wildfire variability using recently created multicentury proxy indices of SAM for the years 1531–2010 AD. We show that at interannual time scales, as well as at multidecadal time scales across 37–54 °S, latitudinal gradient elevated wildfire activity is synchronous with positive phases of the SAM over the years 1665–1995. Positive phases of the SAM are associated primarily with warm conditions in these biomass-rich forests, in which widespread fire activity depends on fuel desiccation. Climate modeling studies indicate that greenhouse gases will force SAM into its positive phase even if stratospheric ozone returns to normal levels, so that climate conditions conducive to widespread fire activity in SAS will continue throughout the 21st century.

fire scars | climate modes | AAO | synchrony | warming

Fire is a key ecological process in southern South America (SSA) that affects ecosystem dynamics and services (1) and smoke-related human health (2). Fire activity in SSA is driven primarily by variations in fuel amount and condition, ignition patterns, and climate variability (3, 4). In SSA, wildfire activity is related to large-scale climate modes, such as the El Niño-Southern Oscillation (ENSO), as evidenced in landscape-scale tree ring fire histories typically spanning ∼2° of latitude (5–7) and in modern documentary fire records across biomes ranging from semiarid to rainforest ecosystems (3). Understanding fire–climate relationships can clarify the relative importance of humans in either increasing or decreasing wildfire activity, and help land managers better anticipate future fire activity under climate change (3). To date, however, there have been no broad-scale syntheses of long-term (i.e., multicentury) fire activity and climate–fire dynamics for any region in the Southern Hemisphere.

Since the 1950s, there has been a rise in temperature during the growing season at mid to high latitudes in the Southern Hemisphere (Fig. 1*A*), a phenomenon largely attributed to an intensification and poleward shift in the Southern Hemisphere westerlies- associated variability of the Southern Annular Mode (SAM) (8–11) (Fig. 1*B*). During this period, the SAM has experienced an upward (positive) trend during spring and summer (Fig. 1*C*), attributed to stratospheric ozone depletion and increases in greenhouse gases (12), which is unprecedented over the last 1,000 y (13). The leading pattern of tropospheric circulation variability south of 20 °S, the SAM is essentially a zonally symmetric or annular structure with synchronous, seesaw-like anomalies of opposite signs in Antarctica and the midlatitudes (∼40–50°S) (8). During the SAM's positive phase, decreased (increased) surface pressure and geopotential heights are observed over Antarctica (midlatitudes) and the southern westerly winds strengthen and shift poleward, while opposite conditions prevail during its negative phase (8, 14). For SSA, this SAM-mediated increase in surface pressure and geopotential heights acts like a blocking pressure system that since the 1950s has been associated with (*i*) warmer conditions due to a combination of enhanced horizontal advection, subsidence, and solar radiation (15), particularly south of 40 °S and during the summer (14), and (*ii*) dry conditions due to reduced frontal and orographic precipitation (16) and weakening of the moisture convergence (17), particularly at 40°S and in the spring (14).

The SAM has been shown to be a major driver of fire activity across the broad range of ecosystem types, from semiarid to rainforest ecosystems, based on short (1984–2010) documentary fire records (3) and over a centennial time scale (ca. 1800 to the

Significance

Fire is a key ecological process affecting ecosystem dynamics and services, driven primarily by variations in fuel amount and condition, ignition patterns, and climate. In the Southern Hemisphere, current warming conditions are linked to the upward trend in the Southern Annular Mode (SAM) due to ozone depletion. Here we use tree ring fire scar data obtained from diverse biomes ranging from subtropical dry woodlands to sub-Antarctic rainforests to assess the effect of the SAM on regional fire activity over the past several centuries. Our findings reveal a tight coupling between fire activity and the SAM at all temporal scales and in all biomes, with increased wildfire synchrony and activity during the 20th century compared with previous centuries.

Author contributions: A.H., J.P., and T.T.V. designed research; A.H. performed research; A.H., T.T.V., and G.J.W. analyzed data; A.H., J.P., I.A.M., T.T.V., T.K., E.A., C.B.-S., M.E.G., H.R.G., and J.M.Q. provided fire scar data and A.H., J.P., I.A.M., T.T.V., and T.K. interpreted results; and A.H. and T.T.V. led the writing of the paper, and all authors contributed substantially to revisions.

The authors declare no conflict of interest.

This article is a PNAS Direct Submission.

Data deposition: The tree-ring fire scar data reported in this paper have been deposited in the International Tree-Ring Data Bank (ITRDB), https://www.ncdc.noaa.gov/data-access/paleoclimatology-data/datasets/tree-ring.

[1]To whom correspondence should be addressed. Email: andres.holz@pdx.edu.

This article contains supporting information online at www.pnas.org/lookup/suppl/doi:10.1073/pnas.1705168114/-/DCSupplemental.

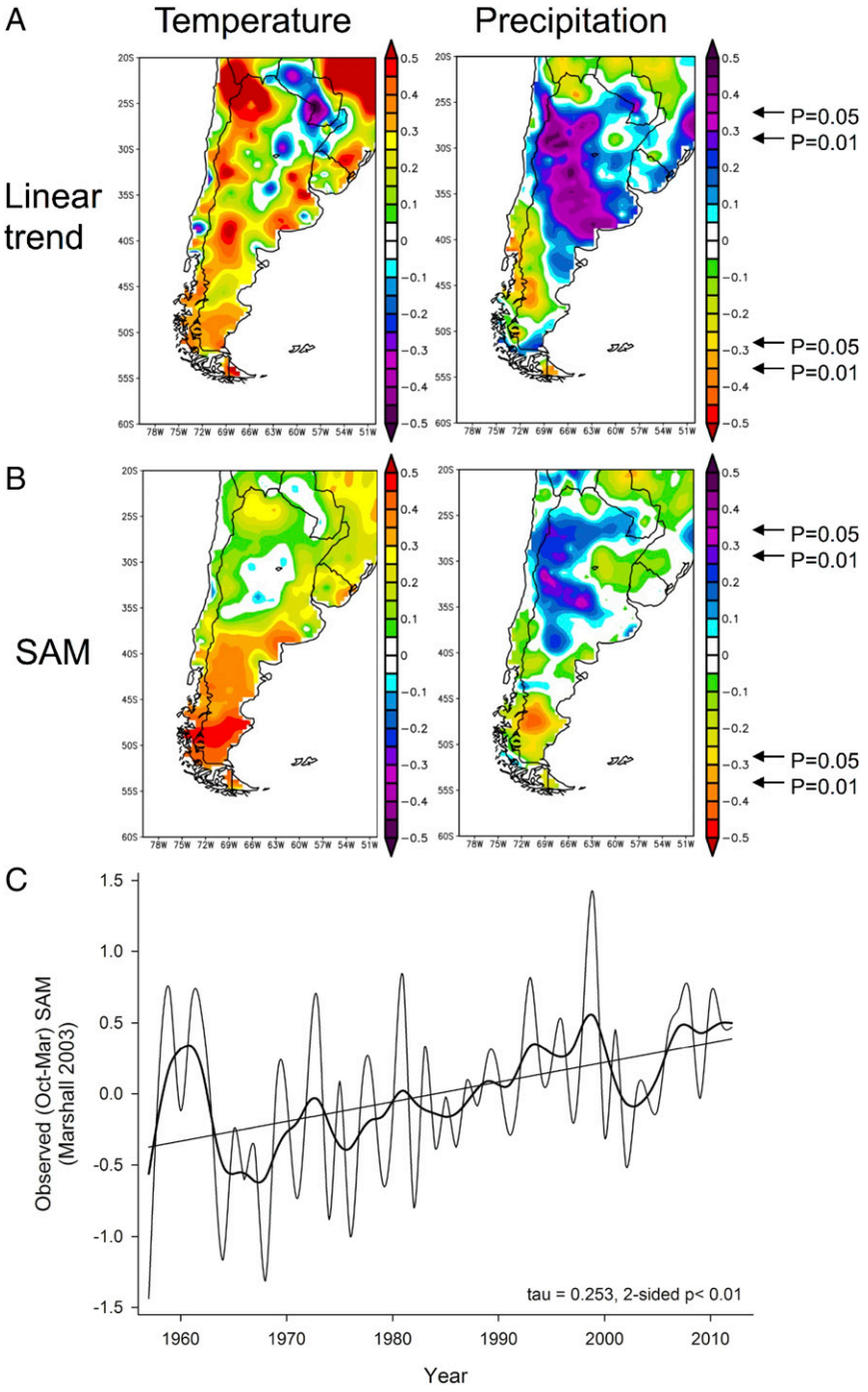

Fig. 1. Modern trends and teleconnections of climate and the SAM in SSA. (*A* and *B*) Spatial correlation between observed precipitation and temperature (gridded July–February data; University of Delaware) with a linear time series (i.e., 1, 2, 3. . .) for the 1949–2008 period (*A*) and observed (July–February) SAM for the 1957–2008 period (*B*). (*C*) Mean spring–summer (October–March) values of the observed SAM for 1957–2012 (9, 12); www.nerc-bas.ac.uk/icd/gjma/sam.html. Significant correlation ($P < 0.05$ and < 0.01) are indicated with arrows in *A* and *B*. In *C*, a linear fit and low-pass Gaussian filter (bold line) highlight the low-frequency trend (11-y window), and values for Kendall's τ statistic and two-sided *P* values are shown. The series was also tested for lag-1 correlation, which was found to be nonsignificant ($P > 0.05$).

present) for specific forest types based on tree ring fire histories (7, 18). However, we lack a comprehensive understanding of the SAM's influence on fire activity over multiple centuries and at a broad latitudinal extent of forest ecosystems in SSA. We hypothesize that in biomass-rich temperate forests extending from ~37° to 55° S in SSA, the SAM promotes fire primarily by enhancing warm spring-summer conditions, which in turn desiccate fuels. Here we used 4,587 annually resolved fire scar dates from 1,767 fire-scarred trees collected at 97 sites (the largest paleofire record yet assembled for the Southern Hemisphere) to reconstruct regional fire records for eight regions that extend from subtropical to sub-Antarctic latitudes in SSA and span the period 990–2010 AD (Fig. 2*A* and *SI Appendix*, Fig. S1 and Table S1). From these fire scar dates, we developed indices of regional- and subcontinental-scale fire activity and synchrony to examine relationships between the SAM and local and regional climate parameters across SSA at

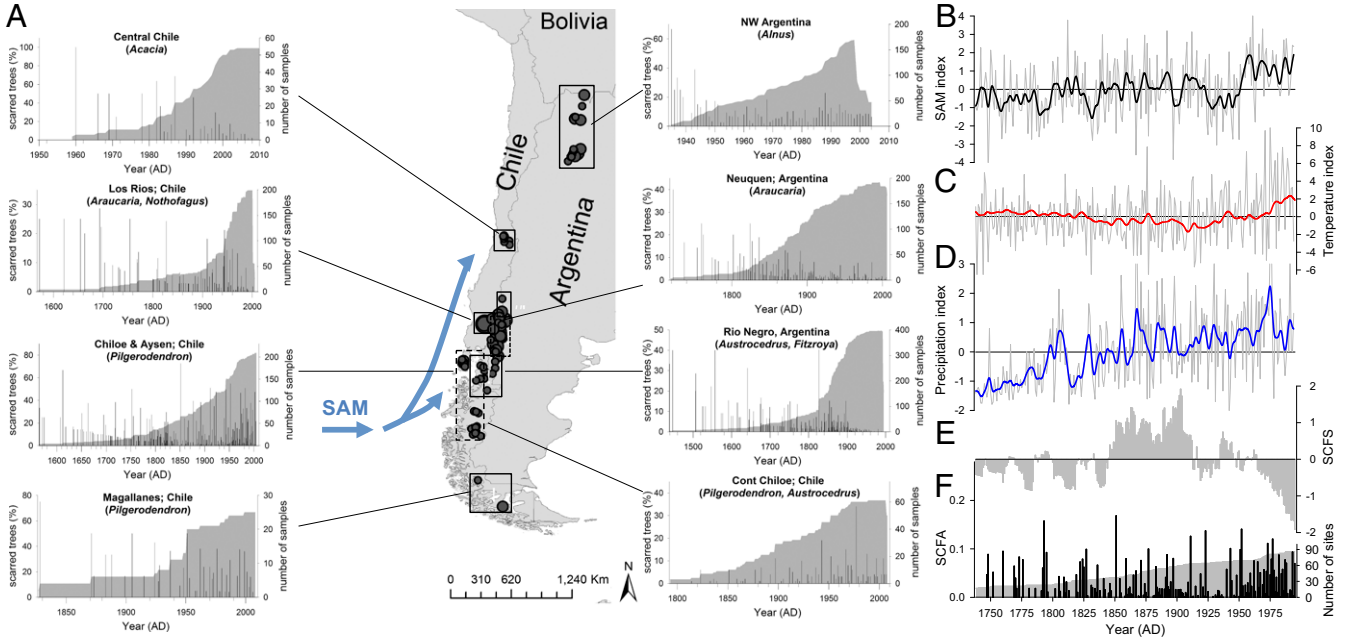

Fig. 2. Tree ring-based fire history and study regions (97 sites and 1,767 fire scars) in SSA. Study region locations (boxes) and primary sampled species (in parentheses) are indicated. Histograms show the fire-scarred trees (%; vertical bars on the left *y* axis) and sample depth (gray area on the right *y* axis; starting when ≥3 trees per region had been scarred at least once); note that the *x*- and *y*-axes are not scaled equally in each region (*A*). Light-blue arrows indicate the geographical domain of the dominant extratropical forcing of regional climate variability, as represented by the SAM. The number of sites sampled within each region is indicated by the size of the black circles on the map. Graphs in the far right column show reconstruction of the SAM index departures (December–February; Marshall, black line) (26) (*B*), temperature departures (mean annual reconstruction for the Southern Hemisphere; red line) (28) (*C*), precipitation departures (total December–February SSA reconstruction; blue line) (27) (*D*), SCFS departures (gray bars; 15-y moving averages) (*E*), and SCFA (black bars) and total number of search sites (i.e., sample depth; gray fill) (*F*). All climate series and the SCFS were standardized (*z*-scores, in SD units), detrended, and prewhitened. All annually resolved climate series (light-gray lines) were smoothed with a 15-y spline. Records from northwestern Argentina and central Chile were not used in building the subcontinental fire indices owing to their short sample depth.

multiple time scales. Our rationale is that at the regional and subcontinental scales, high synchrony indicates a strong influence of climatic variations on fire (19), and that overall high fire activity could have a strong association with climate variability (19–21) as well as with changes in ignition owing to either natural (22) or human (23–25) causes.

We used a recently developed proxy reconstruction of summer (December–February) SAM (9, 26) to examine the relation of fire activity to variability in the SAM (*Methods*). This SAM reconstruction has proven useful in explaining tree growth variability in much of our study area (26). We also tested for the influence of variabilities in precipitation and temperature on fire activity at multiple scales, using proxy reconstructions of precipitation for SSA (27) and of temperature for the Southern Hemisphere (precipitation index and temperature index hereinafter) that are heavily weighted by the Pacific sector of the Southern Hemisphere and thus suitable for our study area (28).

Results and Discussion

Reconstructed mean values of the SAM during years of widespread fire (no fire) are significantly above (significantly or trend below) the long-term mean in all study regions located south of 37°S (*SI Appendix*, Figs. S2 and S3 and Text ST1). During the period of the instrumental records (1957–2013), higher (lower) SAM values are correlated with higher (lower) temperatures and reduced (increased) precipitation in most seasons of the year, including the fire season (*SI Appendix*, Fig. S4). In all study regions south of 37 °S in SSA, the overall pattern is one of increased fire activity driven by fuel desiccation, rather than by insufficient quantity of fine fuel (*SI Appendix*, Text ST1), associated with a positive SAM, which closely coincides with and is supported by results and interpretations from modern burned area–climate relationships in woody vegetation over the 1984–2010 period (3).

The collective fire history of all study regions' chronologies south of 37 °S combined (minimum of two trees and 10% of recorder trees per site) shows a rapid decline from early in the record (1400s) to the 1700s, when fire activity increased gradually (*SI Appendix*, Fig. S1). Starting in the 1850s, fire activity increased very abruptly, and large fire years occurred roughly every 15–20 y until the 1920–1940s, when fire activity dropped. Starting in the 1960s, fire activity ramped up again and has continued to the present day (*SI Appendix*, Fig. S1). The temporal pattern of the collective fire history of all regions is similar to the standardized synthesis of all charcoal records located south of 30 °S in western South America (29). The post-1960s increases in fire activity has been driven primarily by fire activity at mid and high latitudes on the west side of the Andes (Fig. 2*A*), where wildfires on the eastern Andean slope show the effects of active fire suppression since the 1930s–40s (Fig. 2*A*). The subcontinental-scale fire indices indicate that both the magnitude of fire activity (SCFA) and fire synchrony (SCFS) among regions have fluctuated over time and that in general there is no clear relationship between these two indices (Fig. 2 *E* and *F*). In contrast to the SCFA index, the amplitude in the SCFS index has increased over time, with higher maximum values and lower minimum values in the latter part of the analyzed period (1738–1932) compared with early in the record.

Relatively weak but significant correlations were found for both subcontinental fire indices (SCFA: $r = 0.2$, $P < 0.01$; SCFS: $r = 0.18$, $P < 0.01$) and the SAM during the 1738–1932 period (Table 1). Series were prewhitened to remove autocorrelation, and the trend-free records were filtered with a 15-y spline to match the main spectra of the SCFA (*SI Appendix*, Fig. S5). Likewise, similar low-frequency variability patterns were shared between the temperature

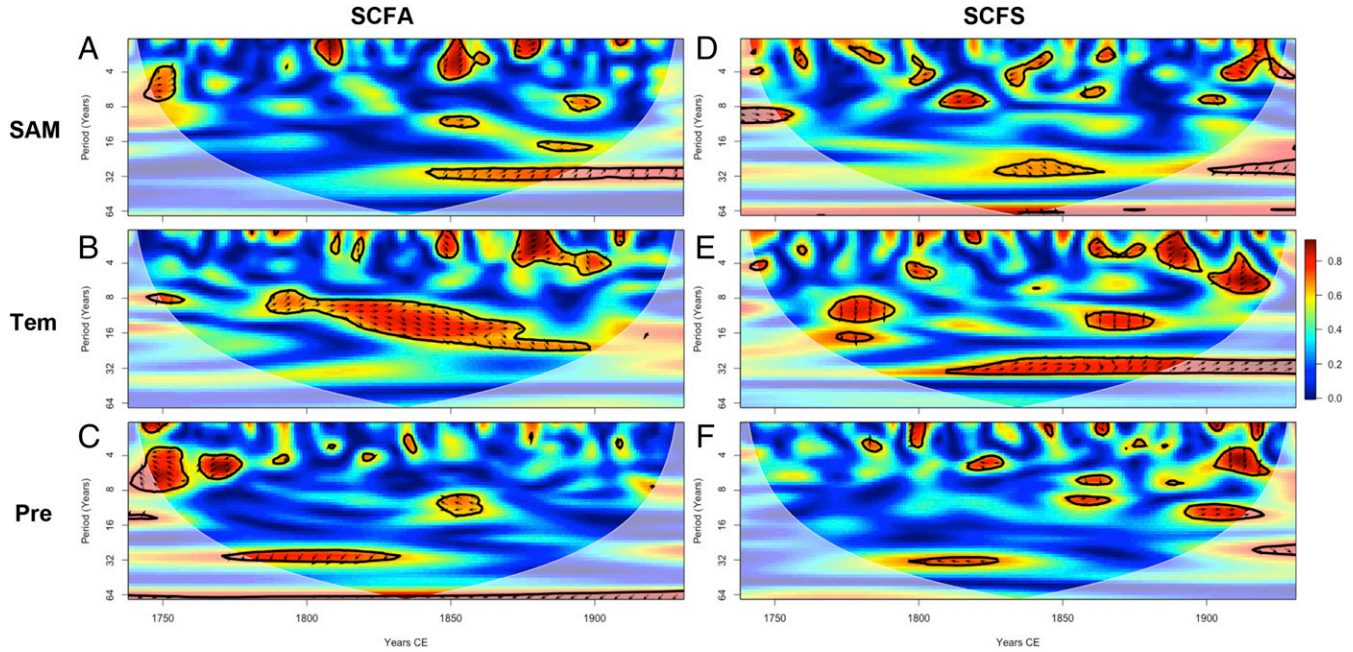

Fig. 3. Wavelet coherence between climate and fire at the subcontinental scale (SCFA, *Left*, and SCFS, *Right*) and SAM (*A* and *D*) temperature (*B* and *E*), and precipitation (*C* and *F*) index reconstructions. Red regions in the plots indicate the frequencies and times for which pairs of series were coherent. The cone of influence (white dashed line) and the significant coherent time-frequency regions ($P < 0.01$; 1,000 Monte Carlo simulations; black solid line) are indicated. All figures were computed using standardized (i.e., *z*-scores) series that were detrended and prewhitened (*Methods*). Data sources: SAM (December–February), (9); temperature index (mean annual reconstruction for the Southern Hemisphere), (28); precipitation index (total December–February SAS reconstruction), (27).

and SCFA indices ($r = 0.12$, $P < 0.01$) and between the precipitation and SCFS indices ($r = 0.24$, $P < 0.01$) (Table 1).

The patterns of wavelet coherence between the SCFA and both the SAM and temperature indices show numerous shorter (ca. four 2–8 y) and longer (ca. two 10–18 y) periods with either in-phase and/or delayed in-phase coherence throughout the recording period (Fig. 3 *A* and *B* and *SI Appendix*, Text ST1). Similarly, the SCFS and SAM indices share similar common numerous short (ca. 4–8 y) and a few longer (ca. 8–12-y) periods with either in-phase and/or delayed in-phase coherence (Fig. 3*D*). Some of the short period coherence might reflect the linkage of fire and the climatic parameters to ENSO variability documented in previous studies (5–7, 30, 31); however, the goal of the present analysis was to identify the SAM signal in the coherence patterns. Only decadal-scale in-phase and/or delayed in-phase coherence (ca. 28–34 y) is shared between SCFS and temperature (Fig. 3*E*). The precipitation index and both fire indices share mostly antiphase or delayed antiphase coherence (i.e., drought and fire), with common numerous short (ca. 1–8 y) and fewer longer (ca. 8–10 y) periods (Fig. 3 *C* and *F*). Precipitation also shares a few common in-phase and/or delayed in-phase coherence of longer (ca. 10–16 y) periods with the SCFS (Fig. 3*F*). Overall, wavelet coherence analyses on the SCFA also show a predominant role of drought in the first third of the record (i.e., 1738–1825), with the SAM and temperature indices increasing in relevance over the remaining record (Fig. 3 *A*–*C*). Similarly, an increase in coherence between the precipitation and SCFS indices is also observed from the 1780s to 1930s (Fig. 3*F*), but no obvious change in coherence over time is noted between the SCFS and either the SAM or temperature index (Fig. 3 *D* and *E*).

The foregoing results indicate that at the subcontinental-scale, large wildfire years (SCFA) were driven primarily by warm conditions teleconnected with a positive SAM during 1738–1932. Some years of high synchrony in subcontinental fire activity are linked to reduced rainfall. In both cases, our rationale in interpreting these results is that in SSA [and elsewhere (19, 20, 32)], large fire years in cool and/or wet forests with abundant fuels and a short fire season have been commonly associated with periods of warm and dry conditions that reduce fuel moisture and favor fire activity. We speculate that the association between high fire synchrony and above-average precipitation reflects the spread of fires that began in fuel-limited grasslands adjacent to the core areas sampled for fire scars, where previous research had shown a lagged association of fire and fine fuel-enhancing moister conditions (5, 33). This interpretation is consistent with the lagged association of fire with above-average moisture availability in grassland habitats throughout SSA based on modern climate-fire analyses using instrumental climate records and observations of annual area burned (3).

The peaks in fire activity in the mid-1800s and early 1900s have been linked to coincident increases in human-set fires and climate variability in some of our study regions (6, 34, 35). While increases in fire frequencies in association with the increased presence of

Table 1. Pearson correlation values of 15-y smoothed time series (z-scores) of climate and fire (SCFA and SCFS) over the 1738–1932 period (n = 194)

Series	*r* value
SCFA vs. SAM	0.20***
SCFA vs. temperature	0.12*
SCFA vs. precipitation	−0.09
SCFS vs. SAM	0.18**
SCFS vs. temperature	−0.05
SCFA vs. precipitation	0.24***
SCFA vs. SCFS	0.07

All reconstructions were filtered with a 15-y spline to emphasize the correlations among the low frequency of all records. All time series were detrended. Pearson correlation coefficients were calculated from prewhitened series using the trend-free prewhitening procedure in the zyp R package. The subcontinental fire indices were built using a constant number of fire recording sites over the 1738–1932 period. *$P < 0.05$; **$P < 0.01$; ***$P < 0.001$.

indigenous and modern humans are detectable in specific habitats, periods of synchronous widespread fire documented at annual resolution in tree ring studies and at multidecadal resolution in sedimentary charcoal studies have been more strongly linked to climatic variability (4, 6, 34). Human amplification or dampening of climate-induced trends in wildfire activity would not have been synchronous across the six study areas, given different time periods of migrations of indigenous populations and colonization by populations of European origin until the 1930s–1940s, when fire records in some regions clearly reflect fire exclusion (e.g., ref. 7), but records in other regions reflect increased burning by modern humans (34). Thus, we use 1932 as a cutoff to reduce the impact of modern changes in human ignition (Fig. 2 *A* and *F* and *Methods*) while acknowledging that in some regions, pre-1932 human amplification and/or changes in lightning activity (1, 36) might have affected both subcontinental-scale indices (SCFA and SCFS).

Conclusions and Implications

In SSA, wildfire activity is strongly associated with warm conditions teleconnected with positive a SAM at multiple time scales both within large areas defined by specific forest ecosystem types and at subcontinental scales across a broad range of forest ecosystem types. At an interannual time scale, widespread fires across SSA co-occurred during anomalously high SAM conditions over an extensive north-to-south gradient at ∼37–54°S, based on 1,252 scarred trees at 71 sites. Across this latitudinal range, most study sites are dominated by forests ranging from moderate- to high-density stands in which fuel quantity is not limiting to fire occurrence and instead years of widespread fire depend on fuel desiccation (*SI Appendix*, Text ST1). Ice cores and other proxies from Antarctica and SSA show that the positive trend in the SAM since the 1940s is at its highest level over at least the past 1,000 y (13), and that atmospheric greenhouse gases will keep forcing the SAM into its positive phase even if stratospheric ozone returns to normal levels (12, 37). Atmospheric greenhouse gases are also expected to force more frequent extreme El Niño events (38), which have been shown to be strongly associated with years of large wildfire activity in SSA (mainly north of 44°S) both directly and in combination with a positive SAM at the intraregional scale (*SI Appendix*, Tables S2 and S4). During the 2016–17 fire season, more than 500,000 hectares affected in the zone between ∼29 °S and 40 °S (∼3–5% of only that latitudinal zone) were burned in central and southern Chile, driven by a long-lasting drought that was amplified by concurrent positive SAM and ENSO conditions. While wildfire activity is expected to continue to reflect interannual variability related to ENSO, the continued dominance of the SAM as the primary driver of extratropical climate variability in the Southern Hemisphere (11, 37) portends increased wildfire activity in SSA for the 21st century.

Methods

Study Sites and Species. Tree ring fire scar records were obtained from the International Multiproxy Paleofire Database (IMPD), and from published and unpublished sources (*SI Appendix*, Table S1). This dataset consists of 1,767 fire-scarred trees from 97 sites in SSA extending from northwestern Argentina to southern Patagonia, which were grouped into eight regions of homogeneous climate variability (Fig. 2*A*) (following ref. 3). Included ecosystems range from relatively dry woodlands and forests to mesic and rain forests and bogs.

Indices. We created regional- and subcontinental-scale indices of years of fire activity to highlight and test for changes at interannual and decadal scales. Annual indices of fire occurrence (i.e., fire index) were calculated for each of the 97 sites by dividing the number of fire-scarred trees per year (with a minimum of two) by the number of trees potentially recording fire in that year, as described previously (24, 39). The start and end dates for each site fire index were determined using a minimum of four samples capable of recording fire. A region-wide fire index (for each of our eight regions) was then calculated as the sum of the site indices per year divided by the number of sites recording fire in that year (*SI Appendix*, Table S3). The SCFA was then calculated as the sum of the regional fire indices per year divided by the number of regions recording fire in that year (Fig. 2*F*).

For the SCFS, in a modification of a previously described method (19), annual fire synchrony between paired regions was identified by calculating the number of fire years recorded in both regions divided by the number of fire years recorded in either region over a centered 15-y period. This procedure was repeated in the 15 possible combinations of pairs of the six regions (the records for the two northernmost regions were too short and thus were not included) and summed as total fire synchrony, or SCFS (Fig. 2*E*).

A cutoff date of 1738 was chosen for all statistical analyses (see below) to ensure a minimum sample of recording sites ($n = 8$; >10%), a sufficient and commonly used percentage to characterize fire regimes in SSA (6, 7, 18, 30, 31). In addition, the time period of analysis ends in 1932, when both the earliest known effective fire suppression in SSA is evident in the fire records of the Río Negro and Neuquén regions, and a pulse of fire activity is initiated in the 1940s in the Aysén region associated with modern frontier activity and road construction (Fig. 2*A* and *SI Appendix*, Tables S1 and S3).

The annually resolved reconstructions of the SAM (Fig. 2*B*), the Southern Hemisphere temperature index (28) (Fig. 2*C*), and the SAS precipitation index (27) (Fig. 2*D*) were obtained from the paleoclimatology datasets of the National Centers for Environmental Information (https://www.ncdc.noaa.gov/data-access/paleoclimatology-data/datasets/climate-reconstruction). The SAM reconstruction was developed from tree ring records, and the temperature and precipitation reconstructions were developed from tree rings, marine and lake sediments, ice cores, documentary, coral and speleothem records (*SI Appendix*, Text ST1). Several SAM reconstructions have been developed (13, 26), all of which share some of the same proxies (e.g., tree ring chronologies) and thus are not independent reconstructions. We chose to use the SAM [based on the Marshall Index (9)] reconstruction because (*i*) the instrumental index used to build the SAM reconstruction is based on sea-level atmospheric pressure records from stations located between 40 °S and 65 °S, rather than on reanalysis data (SAM NCEP-NCAR), which has been shown to magnify the increase in the SAM signal over the past decades (9); (*ii*) the region (40–65 °S) used to build the index is more relevant to our study area than locations of proxies used in other reconstructions (13, 26); (*iii*) in the study areas, the summer season (i.e., December–February) of the SAM reconstruction is strongly correlated with summer weather, which is the key variable affecting fuel desiccation (13); and (*iv*) analyses based on an alternative SAM reconstruction [SAM-NCEP (26)] built from seasonal (December–February) indices are very similar (data not shown).

Seasonal subsets of monthly gridded precipitation and temperature (0.5 × 0.5 degrees; Climate Research Unit TS3.22; 1901–2013) data used to conduct bootstrapped correlation functions (see below) were derived for each study region as defined by the boxes in the map shown in Fig. 2*A*. The instrumental index of the SAM used was Marshall's summer (December–February) index (9), which is based on selected station pressure records for 40–65 °S over the period 1957–2013. This instrumental SAM index is strongly correlated with tree growth in SSA (26).

Statistical Analyses. We performed three analyses to examine the spatiotemporal associations between wildfire activity in SSA and variability in the SAM, precipitation, and temperature index reconstructions. First, at the regional scale, we determined interannual-scale departures from long-term mean SAM during periods of widespread fire and nonfire years in each of the study regions using superposed epoch analysis (SEA) (33) in the dplR package (40) in R (41) (*SI Appendix*, Fig. S2). For the SEA, years of widespread fire within each study area were defined as years when ≥2 trees were scarred, with a minimum of four trees capable of recording fire per site at ≥10% of sites (i.e., region-wide fire index for each of our eight regions). A 5-y window of mean SAM was centered on years of widespread (and no fire scars; *SI Appendix*, Fig. S3) fires for each of the study regions. Significance levels of the departures from the long-term mean were determined from bootstrapped 95% confidence intervals estimated from 10,000 Monte Carlo simulations (42). Modern teleconnections of the instrumental SAM index to local climate variability (mechanistically responsible for variability in wildfire activity) were examined with bootstrapped correlation functions using the bootRes package (43) relating the observed SAM and seasonal gridded climate data for each of the eight study regions (as defined by boxes in the map shown in Fig. 2*A* and *SI Appendix*, Fig. S4). The results of this first analysis were compared with those obtained from modern relationships (significant correlation; $P < 0.05$) between seasonal observations of both climate parameters and SAM and annual area burned in woody vegetation during the 1984–2008 period (results from ref. 3 and *SI Appendix*, Table S4).

Secondly, at the subcontinental scale, wavelet coherence was used to test whether fire activity and climatic parameters had similar periodicities, using the

Biwavelet package in R. Wavelet coherence, which identifies regions in time and space in which two variables covary, is especially suitable for the analysis of non-Gaussian time series, including climate and fire data (32). The Morlet continuous wavelet transform was applied, and the data were padded with 0s at each end to reduce wraparound effects (44). We plotted phase arrows indicating the direction of the correlation only when the wavelet coherence power exceeded the 90th percentile (Fig. 3). Although we found no difference in the coherence patterns compared with analyses conducted using standardized (*z*-scores) time series alone or standardized and detrended time series, before conducting wavelet analyses, we standardized time series (to *z*-scores) and removed trends and serial autocorrelation using autocorrelation functions and autoregressive moving average models (trend-free, prewhitened) using the Yue-Pilon method (45) in the zyp package in R.

Third, and also at the subcontinental scale, we used the Spearman correlation function to test the long-term (decadal-scale) relationships among the reconstructed SAM, the climate parameters, and both subcontinental fire indices (SCFA and SCFS) (Table 1). To highlight decadal-scale variability in climate-fire relationships, we used singular spectral analysis to determine the dominant periods at which variance occurred in the SCFA index (46); specifically, we used the multitaper method (47) to identify a window of 15 y as a cycle that explains significant proportions of variance in the SCFA over the 1738–1932 period (*SI Appendix*, Fig. S5). We used the 15-y window to construct a smoothed SCFA and the climate time series, as well as to build the SCFS. To ensure that the correlation coefficients computed in this third step were not influenced by changes over time in the sample depth (i.e., number of trees, sites, and regions recording fire), we computed correlation coefficients using a constant sample depth (10% of sites with fire-scarred trees) over time over the 1738–1932 period; that is, once the 10% criterion was achieved, new fire dates from recorder trees starting after 1738 were not added into the regional chronologies.

ACKNOWLEDGMENTS. We thank Nerilie Abram, Eric Oliver, and Tarik C. Gouhier for help with programming codes. This work was supported by the US National Science Foundation (Grants 0956552 and 0966472, to A.H., T.T.V., and J.P.), the Consejo Nacional de Investigaciones Científicas y Técnicas (J.P., I.A.M., and T.K.), the Agencia Nacional de Promoción Científica y Tecnológica (Grants PICT 2012-1891, to I.A.M., and PICT 2012-0949, to J.P.), the Graduate School of the University of Colorado Boulder (A.H. and J.P.), and the Center for Climate and Resilience Research (Comisión Nacional de Investigación Científica y Tecnológica/Fondo de Financiamiento de Centros de Investigación en Áreas Prioritarias/Award 15110009, M.E.G.) and Fondo Nacional de Desarrollo Científico (Grant 1171400, to M.E.G.).

1. Veblen TT, et al. (2011) Adapting to global environmental change in Patagonia: What role for disturbance ecology? *Austral Ecol* 36:891–903.
2. Johnston FH, et al. (2012) Estimated global mortality attributable to smoke from landscape fires. *Environ Health Perspect* 120:695–701.
3. Holz A, Kitzberger T, Veblen TT, Paritsis J (2012) Ecological and climatic controls of modern wildfire activity patterns across southwestern South America. *Ecosphere* 3:1–25.
4. Whitlock C, Moreno PI, Bartlein P (2007) Climatic controls of Holocene fire patterns in southern South America. *Quat Res* 68:28–36.
5. Kitzberger T, Veblen TT, Villalba R (1997) Climatic influences on fire regimes along a rain forest to xeric woodland gradient in northern Patagonia, Argentina. *J Biogeogr* 24:35–47.
6. Veblen TT, Kitzberger T, Villalba R, Donnegan J (1999) Fire history in northern Patagonia: The roles of humans and climatic variation. *Ecol Monogr* 69:47–67.
7. Mundo IA, Kitzberger T, Roig Juñent FA, Villalba R, Barrera MD (2013) Fire history in the *Araucaria araucana* forests of Argentina: Human and climate influences. *Int J Wildland Fire* 22:194–206.
8. Thompson DWJ, Solomon S (2002) Interpretation of recent Southern Hemisphere climate change. *Science* 296:895–899.
9. Marshall GJ (2003) Trends in the southern annular mode from observations and reanalyses. *J Clim* 16:4134–4143.
10. Manatsa D, Morioka Y, Behera SK, Yamagata T, Matarira CH (2013) Link between Antarctic ozone depletion and summer warming over southern Africa. *Nat Geosci* 6:934–939.
11. Gong D, Wang S (1999) Definition of Antarctic oscillation index. *Geophys Res Lett* 26:459–462.
12. Thompson DWJ, et al. (2011) Signatures of the Antarctic ozone hole in Southern Hemisphere surface climate change. *Nat Geosci* 4:741–749.
13. Abram NJ, et al. (2014) Evolution of the Southern Annular Mode during the past millennium. *Nat Clim Change* 4:564–569.
14. Garreaud RD, Vuille M, Compagnucci R, Marengo J (2009) Present-day South American climate. *Palaeogeogr Palaeoclimatol Palaeoecol* 281:180–195.
15. Sen Gupta A, England MH (2006) Coupled ocean-atmosphere-ice response to variations in the Southern Annular Mode. *J Clim* 19:4457–4486.
16. Garreaud RD (2007) Precipitation and circulation covariability in the extratropics. *J Clim* 20:4789–4797.
17. Silvestri GE, Vera CS (2003) Antarctic oscillation signal on precipitation anomalies over southeastern South America. *Geophys Res Lett* 30:2115.
18. Holz A, Veblen TT (2011) Variability in the Southern Annular Mode determines wildfire activity in Patagonia. *Geophys Res Lett* 38:L14710.
19. Trouet V, Taylor AH, Wahl ER, Skinner CN, Stephens SL (2010) Fire-climate interactions in the American West since 1400 CE. *Geophys Res Lett* 37:L04702.
20. Kitzberger T, Brown PM, Heyerdahl EK, Swetnam TW, Veblen TT (2007) Contingent Pacific-Atlantic Ocean influence on multicentury wildfire synchrony over western North America. *Proc Natl Acad Sci USA* 104:543–548.
21. Yao Q, et al. (2017) Pacific-Atlantic Ocean influence on wildfires in northeast China (1774 to 2010). *Geophys Res Lett* 44:1025–1033.
22. Abatzoglou JT, Kolden CA, Balch JK, Bradley BA (2016) Controls on interannual variability in lightning-caused fire activity in the western US. *Environ Res Lett* 11:045005.
23. Abatzoglou JT, Williams AP (2016) Impact of anthropogenic climate change on wildfire across western US forests. *Proc Natl Acad Sci USA* 113:11770–11775.
24. Taylor AH, Trouet V, Skinner CN, Stephens S (2016) Socioecological transitions trigger fire regime shifts and modulate fire-climate interactions in the Sierra Nevada, USA, 1600-2015 CE. *Proc Natl Acad Sci USA* 113:13684–13689.
25. Marlon JR, et al. (2008) Climate and human influences on global biomass burning over the past two millennia. *Nat Geosci* 1:697–702.
26. Villalba R, et al. (2012) Unusual southern Hemisphere tree growth patterns induced by changes in the Southern Annular Mode. *Nat Geosci* 5:793–798.
27. Neukom R, et al. (2010) Multi-centennial summer and winter precipitation variability in southern South America. *Geophys Res Lett* 37:L14708.
28. Neukom R, et al. (2014) Interhemispheric temperature variability over the past millennium. *Nat Clim Change* 4:362–367.
29. Power MJ, et al. (2008) Changes in fire regimes since the last glacial maximum: An assessment based on a global synthesis and analysis of charcoal data. *Clim Dyn* 30:887–907.
30. Holz A, Veblen TT (2012) Wildfire activity in rainforests in western Patagonia linked to the Southern Annular Mode. *Int J Wildland Fire* 21:114–126.
31. González ME, Veblen TT (2006) Climatic influences on fire in *Araucaria araucana-Nothofagus* forests in the Andean cordillera of south-central Chile. *Ecoscience* 13:342–350.
32. Mariani M, Fletcher MS, Holz A, Nyman P (2016) ENSO controls interannual fire activity in southeast Australia. *Geophys Res Lett* 43:10891–10900.
33. Baisan CH, Swetnam TW (1990) Fire history on a desert mountain range: Rincon Mountain Wilderness, Arizona, USA. *Can J For Res* 20:1559–1569.
34. Holz A, Veblen TT (2011) The amplifying effects of humans on fire regimes in temperate rainforests in western Patagonia. *Palaeogeogr Palaeoclimatol Palaeoecol* 311:82–92.
35. Holz A, et al. (2016) Fires: The main human impact on past environments in Patagonia? *PAGES Magazine* 2:72–73.
36. Garreaud RD, Gabriela Nicora M, Bürgesser RE, Ávila EE (2014) Lightning in western Patagonia. *J Geophys Res Atmos* 119:4471–4485.
37. Gillett NP, Fyfe JC (2013) Annular mode changes in the CMIP5 simulations. *Geophys Res Lett* 40:1189–1193.
38. Cai W, et al. (2015) ENSO and greenhouse warming. *Nat Clim Change* 5:849–859.
39. Taylor AH, Trouet V, Skinner CN (2008) Climatic influences on fire regimes in montane forests of the southern Cascades, California, USA. *Int J Wildland Fire* 17:60–71.
40. Bunn AG (2008) A dendrochronology program library in R (dplR). *Dendrochronologia* 26:115–124.
41. R Development Core Team (2016) *A Language and Environment for Statistical Computing* (R Institute for Statistical Computing, Vienna, Austria). Available at www.R-project.org.
42. Mooney CZ, Duval RD (1993) *Bootstrapping: A Nonparametric Approach to Statistical Inference*, Sage University Paper Series on Quantitative Applications to Social Sciences (SAGE Publications, Inc., Newbury Park, CA).
43. Zang C, Biondi F (2013) Dendroclimatic calibration in R: The bootRes package for response and correlation function analysis. *Dendrochronologia* 31:68–74.
44. Torrence C, Webster PJ (1999) Interdecadal changes in the ENSO–monsoon system. *J Clim* 12:2679–2690.
45. Yue S, Pilon P, Phinney B, Cavadias G (2002) The influence of autocorrelation on the ability to detect trend in hydrological series. *Hydrol Processes* 16:1807–1829.
46. Vautard R, Ghil M (1989) Singular spectrum analysis in nonlinear dynamics, with applications to paleoclimatic time series. *Physica D Nonlinear Phenom* 35:395–424.
47. Mann ME, Lees JM (1996) Robust estimation of background noise and signal detection in climatic time series. *Clim Change* 33:409–445.

Supplementary information

List of Appendix files

Fig. S5. Power spectra of the index of Sub-Continental Fire Activity (SCFA, with changing sample depth) using the MultiTaper method (MTM) for the 1738-1932 period.

ST1: Supplementary Text.

a. Caveats and limitations

b. Precipitation reconstructions

c. Delayed wavelet coherence analyses

Supplementary information references

Table S1. Characteristics of all fire chronologies**.**

REGION (country)	Site	Site Code	Search Area (ha)*	Elevation (m)	Lat (S)	Lon (W)	Tree Spp	# wedges	Period (AD)**	Source
NW Argentina	Cerro Bravo	CBR	389	2000-3000	22°15´S	64°46´W	*Alnus acuminata*	39	1980-2003	(1)
NW Argentina	San Andrés	SAN	270	2000-3000	23°07´S	64°55´W	*Alnus acuminata*	4	1943-2003	(1)
NW Argentina	Volcán	VOL	126	2000-3000	23°57´S	65°26´W	*Alnus acuminata*	21	1966-2003	(1)
NW Argentina	Yala	YAL	427	2000-3000	24°05´S	65°29´W	*Alnus acuminata*	51	1935-2003	(1)
NW Argentina	El Centinela	CEN	NA***	1700-2100	24°10´S	65°03´W	*Alnus acuminata*	19	1915-2003	(2), unpublished
NW Argentina	Medina	MED	NA***	1700-2100	26°23´S	65°02´W	*Alnus acuminata*	25	1944-1995	(2), unpublished
NW Argentina	Hualinchay South	HUS	NA***	1900–2300	26°25´S	65°35´W	*Alnus acuminata*	40	1942-1996	(2)
NW Argentina	Hualinchay North	HUN	NA***	1800–2200	26°30´S	65°33´W	*Alnus acuminata*	40	1945-1996	(2)
NW Argentina	Tacifillo	TAF	NA***	1700-2100	26°41´S	65°20´W	*Alnus acuminata*	38	1943-1997	(2), unpublished
NW Argentina	La Quebradita	QUE	249	2000-3000	26°49´S	65°42´W	*Alnus acuminata*	14	1950-2002	(1)
NW Argentina	El Rincón	RIN	136	2000-3000	26°57´S	65°28´W	*Alnus acuminata*	35	1947-2004	(1)
NW Argentina	Quebrada	QPO	NA***	1800–	27°00´S	65°48´W	*Alnus*	60	1948-	(2)

	del Portugués			2300			*acuminata*		1996	
NW Argentina	Los Sosa	SOS	NA***	1700–2200	27°00´S	65°45´W	*Alnus acuminata*	37	1939-1996	(2)
NW Argentina	La Banderita	BAN	NA***	1800–2100	27°20´S	66°00´W	*Alnus acuminata*	88	1947-1996	(2)
Central Chile	Rungue	RG	NA***	713	33°00′S	70°54′W	*Acacia caven*	4	1983-2006	(3)
Central Chile	Cuesta La Dormida	CD	NA***	660	33°04′S	70°57′W	*Acacia caven*	3	1983-2006	(3)
Central Chile	Los Aromos (cultivated area	LAC	NA***	560	33°05′S	70°51′W	*Acacia caven*	6	1983-2006	(3)
Central Chile	Punta de Peuco	PP	NA***	569	33°06′S	70°50′W	*Acacia caven*	5	1983-2006	(3)
Central Chile	Los Aromos (grazing area)	LAG	NA***	570	33°06′S	70°53′W	*Acacia caven*	8	1983-2006	(3)
Central Chile	Lampa	LP	NA***	560	33°16′S	70°54′W	*Acacia caven*	5	1983-2006	(3)
Central Chile	San Ramón.	SR	NA***	895	33°26′S	70°30′W	*Acacia caven*	7	1983-2006	(3)
Central Chile	Rinconada Maipú	RM	NA***	481	33°30′S	70°53′W	*Acacia caven*	6	1983-2006	(3)
Central Chile	Río Clarillo	RC	NA***	911	33°44′S	70°29′W	*Acacia caven*	7	1983-2006	(3)
Neuquén, Arg	Caviahue	CAV	0.2	1683	37°51'S	71°02'W	Araucaria	7	1824-2006	(4)
Neuquén, Arg	Paso del Arco	PAR	14	1433	38°50'S	71°03'W	Araucaria	22	1710-2007	(4)

Neuquén, Arg	Remeco	REM	1	1111	39°04'S	71°20'W	Araucaria	20	1822-2007	(4)
Neuquén, Arg	Ñorquinco	NOR	7	1170	39°09'S	71°15'W	Araucaria	40	1802-2006	(4)
Neuquén, Arg	Ruka Choroy	RUC	4	1270	39°14'S	71°10'W	Araucaria	23	1836-2006	(4)
Neuquén, Arg	Minchén	MIN	6	1287	39°15'S	71°13'W	Araucaria	40	1831-2006	(4)
Neuquén, Arg	Pinalada Redonda	PIN	1	1094	39°18'S	71°17'W	Araucaria	18	1841-2006	(4)
Neuquén, Arg	Rahue1	RA1	8	1463	39°23'S	71°48'W	Araucaria	22	1811-2007	(4)
Río Negro, Arg	Rahue2	RA2	200	920	39°30'S	70°50'W	Austrocedrus	29	1439-1901	(5)
Río Negro, Arg	Nahuel Mapi	MAP	57	1500	39°32'S	71°02'W	Araucaria	31	1441-2006	(4)
Río Negro, Arg	Paso Tromen	TRO	21	1215	39°35'S	71°27'W	Araucaria	23	1772-2006	(4)
La Araucanía, Chi	Los Venados	VEN	200	1300	39°35'S	71°31'W	Araucaria	33	1531-1987	(6)
Río Negro, Arg	Lago Huechulaufquén	LHU	200	900	39°40'S	71°20'W	Austrocedrus	10	1641-1905	(5)
La Araucanía, Chi	Chinay	CHI	200	1310	39°46'S	71°85'W	Araucaria	32	1693-1990	(6)
La Araucanía, Chi	Quillelhue	QUI	4000	1510	39°48'S	71°82'W	Araucaria	144	1446-1990	(7)
La Araucanía,	Tolhuaca	TOL	4000	1100	38°11'S	71°48'W	Araucaria	11	1762-	González et al., unpubl.

Chi									2001	
La Araucanía, Chi	Malalcahuello	MAL	1000	1200	38°24'S	71°34'W	Araucaria	13	2003 2003	González et al., unpubl.
Río Negro, Arg	San Pedro	SPE	200	880	39°50'S	71°05'W	Austrocedrus	6	1757-1854	(5)
Río Negro, Arg	Estancia Collunco	ECO	200	850	39°56'S	71°08'W	Austrocedrus	16	1656-1996	(5)
Río Negro, Arg	Piedra Tromphul	PTR	200	1060	40.12'S	71.43'W	Austrocedrus	15	1645-1957	(5)
Río Negro, Arg	Rio Caleufú	RCA	200	850	40°35'S	71°10'W	Austrocedrus	29	1592-1897	(5)
Río Negro, Arg	Lago Traful West	LTW	200	950	40°40'S	71°30'W	Austrocedrus	26	1897-1943	(5)
Río Negro, Arg	East Rio Limay	ERL	200	1512	40°42'S	71°07'W	Austrocedrus	21	1512-1996	(5)
Río Negro, Arg	Rio Limay North 1	LN1	200	1060	40°42'S	71°09'W	Austrocedrus	49	1634-1980	(5)
Río Negro, Arg	Rio Limay North 2	LN2	200	1060	40°42'S	71°09'W	Austrocedrus	48	1747-1962	(5)
Río Negro, Arg	Lago Traful East	LTE	200	1050	40°43'S	71°10'W	Austrocedrus	16	1830-1996	(5)
Río Negro, Arg	Rio Limay South	LS1	200	1050	40°43'S	71°09'W	Austrocedrus	42	1641-1989	(5)
Río Negro, Arg	Mallin Blest	MBL	200	950	41°00'S	71°55'W	Fitzroya	4	1875-1996	(5)
Río Negro, Arg	Lago Roca	LRO	200	850	41°20'S	71°45'W	Fitzroya	27	1675-1996	(5)

Río Negro, Arg	Laguna Huala Hue	LHU	200	900	41°30'S	71°30'W	Austrocedrus	28	1747-1950	(5)
Río Negro, Arg	La Cascada de la Virgen	CVI	200	850	41°47'S	71°30'W	Austrocedrus	16	1810-1996	(5)
Río Negro, Arg	Valle Rayado	VRA	200	1100	41°50'S	71°40'W	Fitzroya	9	990-1996	(5)
Río Negro, Arg	Cordóm Serrucho	SER	200	750	41°55'S	71°32'W	Austrocedrus	7	1640-1996	(5)
Río Negro, Arg	Lago Epuyén	LEP	200	600	42°15'S	71°20'W	Austrocedrus	17	1772-1996	(5)
Chiloé/Aysén, Chi	P.N. Chiloé	PNC	14	393	42°31'S	74°07'W	Pilgerodendron	7	1718-2004	(8)
Chiloé/Aysén, Chi	Quiao	QUI	88	352	42°37'S	73°59'W	Pilgerodendron	13	1851-2004	(8)
Río Negro, Arg	Lago Rivadavia	LRI	200	800	42°40'S	71°35'W	Austrocedrus	9	1783-1943	(5)
Chiloé/Aysén, Chi	Mallín Martin	MMA	40	27	42°43'S	73°57'W	Pilgerodendron	10	1943-2002	(8)
Chiloé/Aysén, Chi	Camino Pacifico II	CP2	70	301	42°45'S	74°02'W	Pilgerodendron	16	1851-2004	(8)
Chiloé/Aysén, Chi	Camino Pacifico III	CP3	64	300	42°45'S	74°01'W	Pilgerodendron	9	1813-2002	(8)
Chiloé/Aysén, Chi	Camino Pacifico I	CP1	12	285	42°46'S	74°02'W	Pilgerodendron	10	1851-2002	(8)
Chiloé/Aysén, Chi	Gabino	GAB	198	180	42°53'S	73°54'W	Pilgerodendron	8	1943-2002	(8)
Cont. Chiloé, Chi	Chaitén	CAR	7	18	42°58'S	72°42'W	Pilgerodendron	8	1859-2002	This Study

Cont. Chiloé, Chi	El Amarillo	EAM	20	75	43°02'S	72°30'W	Pilgerodendron	9	1851-2002	This Study
Chiloé/Aysén, Chi	Lago Chaiguata	LCH	189	191	43°03'S	73°54'W	Pilgerodendron	7	1943-1952	(8)
Cont. Chiloé, Chi	Cardenas	CAR	9	49	43°06'S	72°28'W	Pilgerodendron	6	1839-2002	This Study
Cont. Chiloé, Chi	Rio Grande	RGR	200	500	43°10'S	71°35'W	Austrocedrus	8	1871-1925	(5)
Cont. Chiloé, Chi	Santa Lucía	CAR	35	552	43°22'S	72°24'W	Pilgerodendron	9	1755-1998	This Study
Cont. Chiloé, Chi	El Aceite	CAR	4	436	43°35'S	71°46'W	Pilgerodendron	6	1892-2007	This Study
Cont. Chiloé, Chi	El Diablo	CAR	4	113	43°35'S	72°04'W	Pilgerodendron	12	1865-2007	This Study
Cont. Chiloé, Chi	La Junta	CAR	25	51	43°58'S	72°25'W	Pilgerodendron	11	1779-2004	This Study
Chiloé/Aysén, Chi	Puerto Raul Marin Balmaceda	PRB	184	5	43°59'S	72°42'W	Pilgerodendron	6	1755-2005	(8)
Chiloé/Aysén, Chi	Queulat	QUE	36	209	44°07'S	73°02'W	Pilgerodendron	6	1824-2005	(8)
Chiloé/Aysén, Chi	Vidal	VID	189	336	44°52'S	72°12'W	Pilgerodendron	7	1614-2005	(8)
Chiloé/Aysén, Chi	Exploradores West	EXW	170	48	46°28'S	73°12'W	Pilgerodendron	11	1834-2005	(8)
Chiloé/Aysén, Chi	Exploradores Central	EXC	142	142	46°31'S	73°02'W	Pilgerodendron	7	1911-2005	(8)
Chiloé/Aysén,	Exploradores	EXE	140	345	46°37'S	72°51'W	Pilgerodendron	11	1736-	(8)

Chi	East								2005	
Chiloé/Aysén, Chi	Lago Casanova	CAS	63	132	47°38'S	72°58'W	Pilgerodendron	7	1676-2004	(8)
Chiloé/Aysén, Chi	Camino Lago Vargas	LVA	16	28	47°41'S	73°02'W	Pilgerodendron	8	1483-2005	(8)
Chiloé/Aysén, Chi	Lalo	LAL	11	20	47°42'S	73°04'W	Pilgerodendron	6	1673-2005	(8)
Chiloé/Aysén, Chi	Cruce Yungay	CYU	15	23	47°45'S	73°15'W	Pilgerodendron	7	1778-2005	(8)
Chiloé/Aysén, Chi	Tortel	TOR	18	21	47°48'S	73°24'W	Pilgerodendron	7	1709-2005	(8)
Chiloé/Aysén, Chi	Entrada	ENT	103	38	48°00'S	73°07'W	Pilgerodendron	8	1542-2005	(8)
Chiloé/Aysén, Chi	Rio Bravo	RBR	115	7	48°02'S	73°01'W	Pilgerodendron	7	1612-2005	(8)
Chiloé/Aysén, Chi	Lago Leal	LLE	19	84	48°06'S	73°08'W	Pilgerodendron	7	1565-2005	(8)
Chiloé/Aysén, Chi	Entrerios	ENR	17	135	48°09'S	73°06'W	Pilgerodendron	4	1822-2005	(8)
Chiloé/Aysén, Chi	KM4	KM4	3	35	48°11'S	73°08'W	Pilgerodendron	7	1823-2002	This study
Chiloé/Aysén, Chi	Rio Pascua	PAS	14	40	48°14'S	73°10'W	Pilgerodendron	8	1752-2005	(8)
Chiloé/Aysén, Chi	Rio Berges	BER	21	35	48°15'S	73°16'W	Pilgerodendron	6	1804-2005	(8)
Chiloé/Aysén, Chi	Chucao	CHU	76	79	48°15'S	73°16'W	Pilgerodendron	5	1915-2005	(8)
Chiloé/Aysén,	Lago Cisnes	CIS	9	280	48°22'S	72°40'W	Pilgerodendron	6	1834-	(8)

Chi									2005	
Magallanes, Chi	Peninsula Antonio Varas	PAV	240	134	51°44'S	72°53'W	Pilgerodendron	11	1936-2004	This study
Magallanes, Chi	Peninsula Brunswick	PBR	108	180	53°45'S	71°00'W	Pilgerodendron	14	1732-2006	This study
		Total	97				Total	1767		

Araucaria, Austrocedrus, Fitzroya and Pilgerodendron refer to *Araucaria araucana, Austrocedrus chilensis, Fitzroya cupressoides, and Pilgerodendron uviferum*, respectively.

*Search area refers to the area (ha)
**Period (AD) is bounded by the oldest fire-scar date (i.e. ≥1 tree) and the most recent fire-recorder year for each individual site.
***NA: this information was not recorded.

Table S2. Summary of published atmospheric teleconnections of ENSO and PDO with wildfires in southern South America.

Climate mode	Region	Dominant vegetation	Fire conducive teleconnection	Fire data	Source
ENSO	NW Patagonia	Xeric Austrocedrus woodlands and forests	Antecedent high rainfall and co-occurring drought	Tree rings	(5, 9)
		Mesic Nothofagus forests	Co-occurring drought		
		Mesic Araucaria woodland	Co-occurring drought		(4)
		Herbaceous vegetation	Antecedent high rainfall	Documentary records	(10)
		Woody vegetation	Co-occurring drought and high temperature		
		Mesic Araucaria-Nothofagus forests	Co-occurring drought and high temperature	Tree rings	(11)
		Herbaceous vegetation	Co-occurring drought	Documentary records	(10)
		Woody vegetation			
	Southern Chile	Herbaceous vegetation	Co-occurring drought and high temperature	Documentary records; charcoal	(10, 12)
		Woody vegetation	Co-occurring drought		
PDO	NW Patagonia	Mesic Araucaria woodland	Co-occurring drought	Tree rings	(4)
PDOxENSO	NW Patagonia	Mesic Araucaria woodland	Co-occurring drought	Tree rings	(4)
ENSOxSAM	NW Patagonia	Mesic Araucaria woodland	Co-occurring drought	Tree rings	(4)
PDOxSAM	Southern Chile	Wet ecotonal Pilgerodendron peatland-forest	Co-occurring drought and high temperature	Tree rings	(13)
	Western Patagonia	Wet ecotonal Pilgerodendron peatland-forest	Co-occurring high temperature	Tree rings	(13)

PDOxENSOxSAM	Southern Chile	Wet ecotonal Pilgerodendron peatland-forest	Co-occurring drought and high temperature	Tree rings	(13)
	Western Patagonia	Wet ecotonal Pilgerodendron peatland-forest	Co-occurring drought and high temperature	Tree rings	(13)

Austrocedrus, Araucaria and Pilgerodendron refer to *Austrocedrus chilensis*, *Araucaria araucana, and Pilgerodendron uviferum*, respectively.

Table S3. Characteristics of the regional fire chronologies analyzed at the interannual-scale (i.e. Superimposed Epoch analysis; Fig. S2). For the SEA, years of widespread fire within each study area were defined as years when ≥ 2 trees were scarred with a minimum of four trees capable of recording fire per site at 10% or more sites (i.e. region-wide fire index for each of our eight regions).

Region	Years of widespread fire	Number of sites	Number of trees	Period
Neuquén	36	10	246	1722-1932
La Araucania	32	3	199	1754-1987
Rio Negro	71	21	432	1447-1932
Continental Chiloe	30	7	61	1836-2004
Chiloe/ Aysen	86	28	221	1695-2004
Magallanes	27	2	93	1793-2004
Total	282	71	1252	

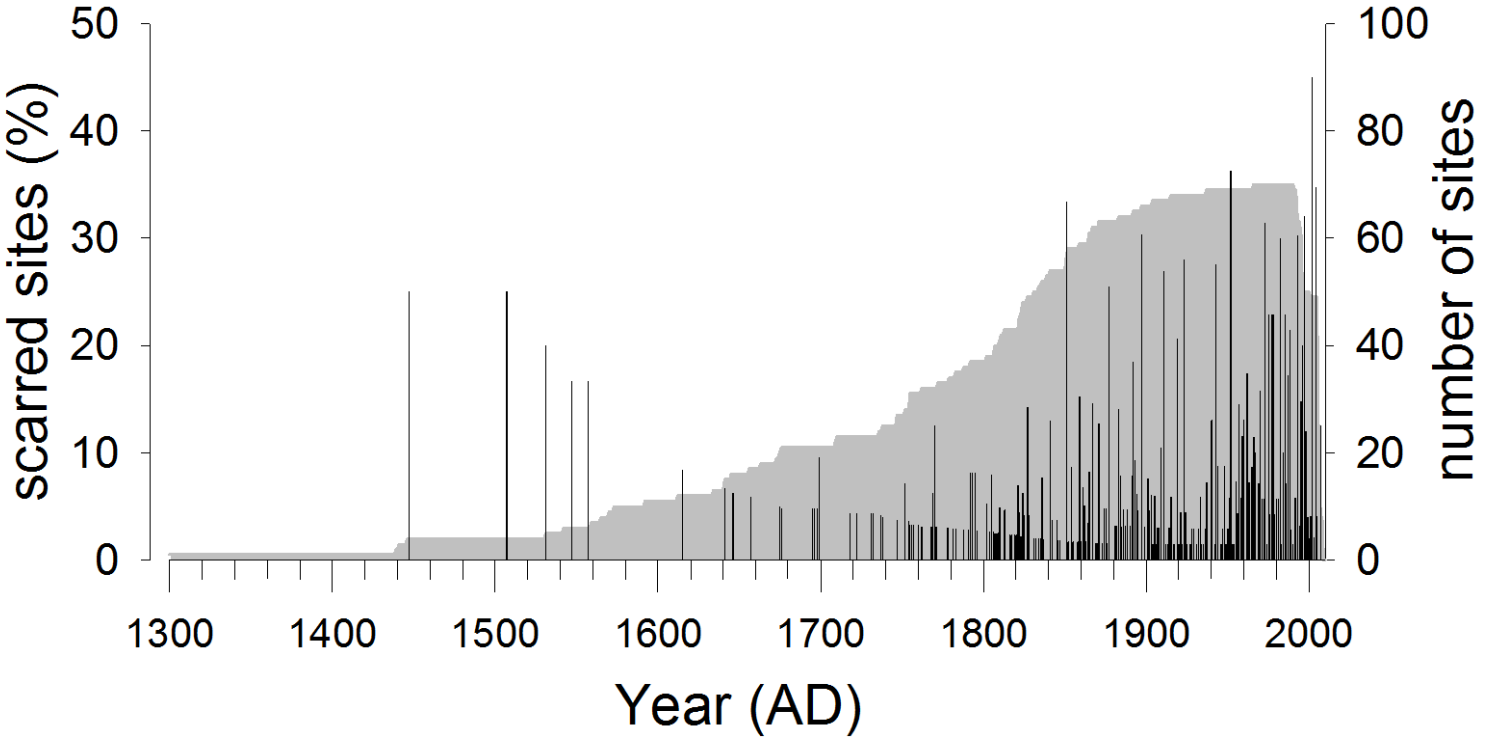

Fig. S1. Percentage of fire-scarred sites (minimum 2 trees and 10% of recorder trees per site; vertical bars) and sample depth (dark grey area) for all six study regions south of 37°S combined during the 1439 – 2010 AD period (i.e. NW Argentina and Central Chile are excluded due to their short record length). Percentage scarred sites is plotted starting with a minimum-sample depth of 3 sites.

Table S4. Summary of modern relationship (significant [$p<0.05$] correlation) between seasonal observations of climate parameters and SAM and annual area burned in woody vegetation over the 1984–2008 period for broad latitudinal zones in SSA (results from (10)).

	Annual Area Burned	
	36-44°S	45-55°S
Precipitation		
Spring	Negative	
Summer		Negative
Temperature		
Spring		Positive
Summer	Positive	
SAM		
Spring	Positive	Positive
Summer	Positive	

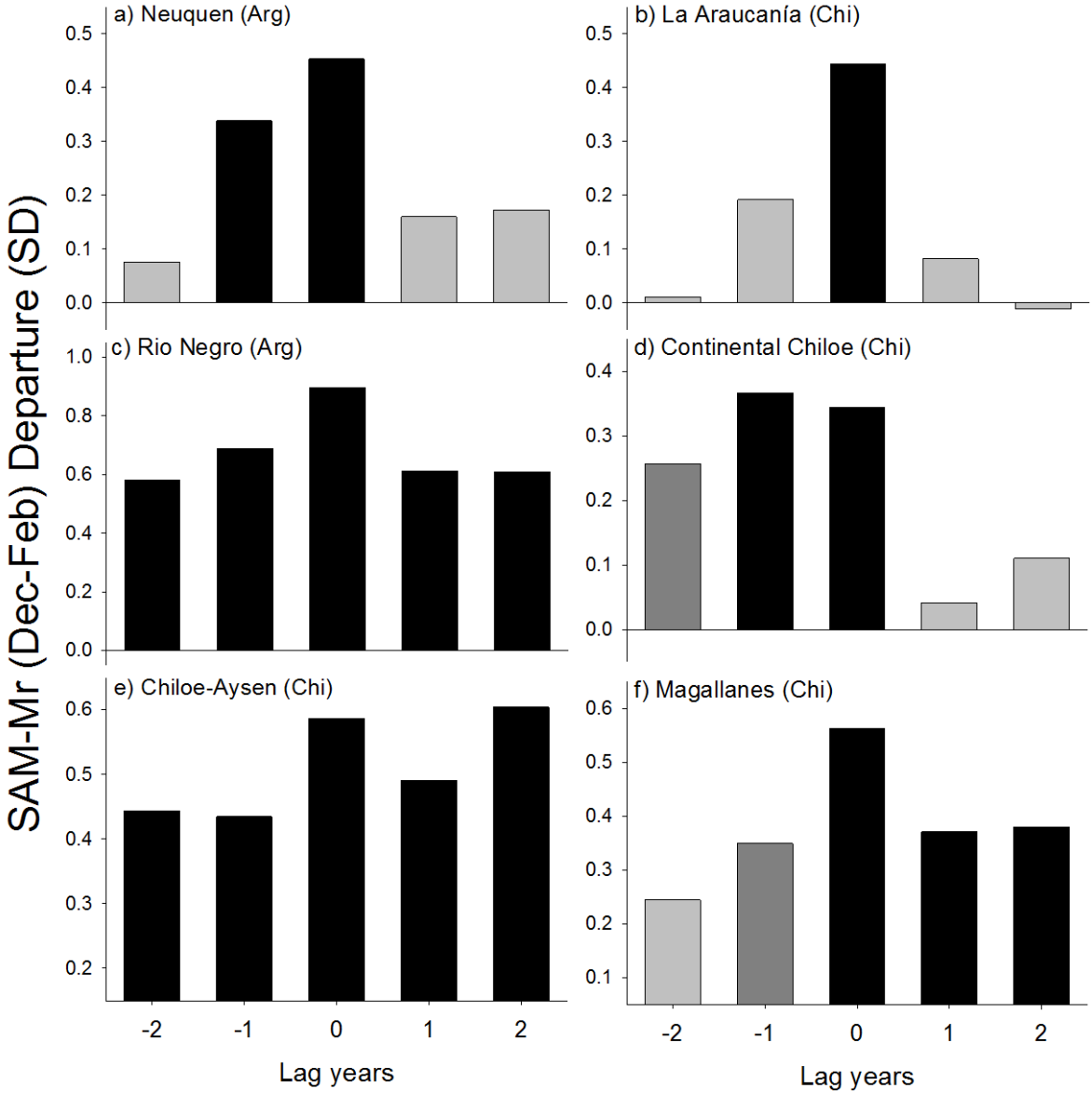

Figure S2. Departures (SDs) from mean values for tree-ring reconstructed indices of SAM-Mr (DJF; Marshall, (14)) for a 5-yr window (t-2 to t+2) centered on years of widespread wildfires in a) Neuquén (Arg) (n= 36 widespread fire years computed from a total of 10 sites & 246 trees over the 1722-1932 period) [see Table S3], b) La Araucanía (Chi) (n= 32 widespread fire years computed from a total of 3 sites & 199 trees over the 1754-1987 period), c) Río Negro (Arg) (n= 71 widespread fire years computed from a total of 21 sites & 432 trees over the 1447-1932 period), d) Continental Chiloé (Chi) (n= 30 widespread fire years computed from a total of 7 sites & 61 trees over the 1836-2004 period), e) Chiloé/ Aysén (Chi) (n= 86 widespread fire years computed from a total of 28 sites & 221 trees over the 1695-2004 period), and f) Magallanes (Chi) (n= 27 widespread fire years computed from a total of 2 sites & 93 trees over the 1793-2004 period). Black and dark grey bars indicate statistically significant (derived from 10000 Monte Carlo simulations) departures ($p<0.05$) and ($p<0.1$), respectively. Note different scales of the y-axes. Years of widespread fire within each study area were defined as years when ≥ 2

trees were scarred with a minimum of four trees capable of recording fire per site at 10% or more sites (i.e. region-wide fire index for each of our eight regions).

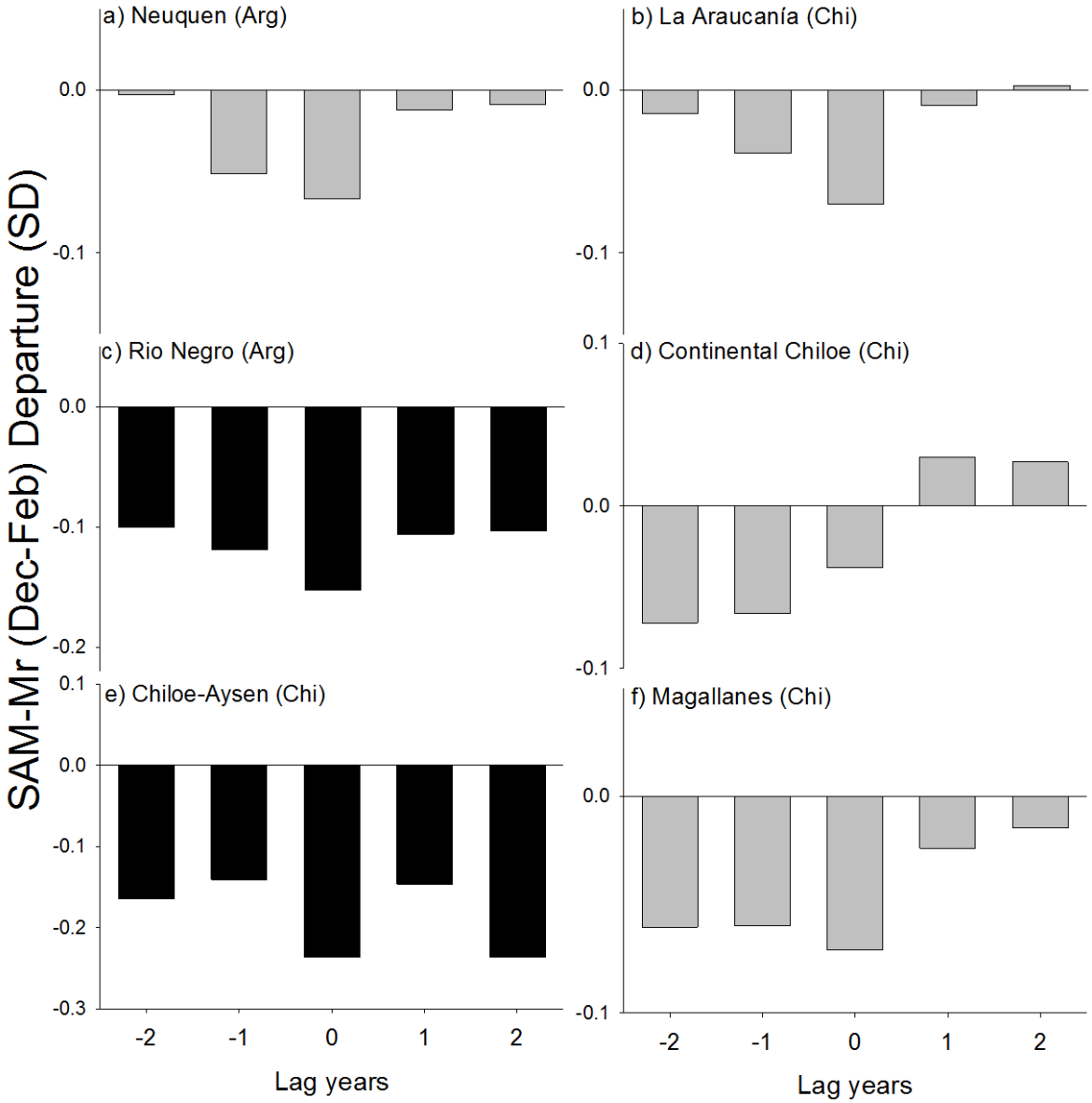

Figure S3. Departures (SDs) from mean values for tree-ring reconstructed indices of SAM-Mr (DJF; Marshall, (14)) for a 5-yr window (t-2 to t+2) centered on years of no fire scars. Periods and non-fire years analyzed per region are as in Fig. S1. Black bars indicate statistically significant (derived from 10,000 Monte Carlo simulations) departures ($p<0.05$). Note different scales of the y-axes.

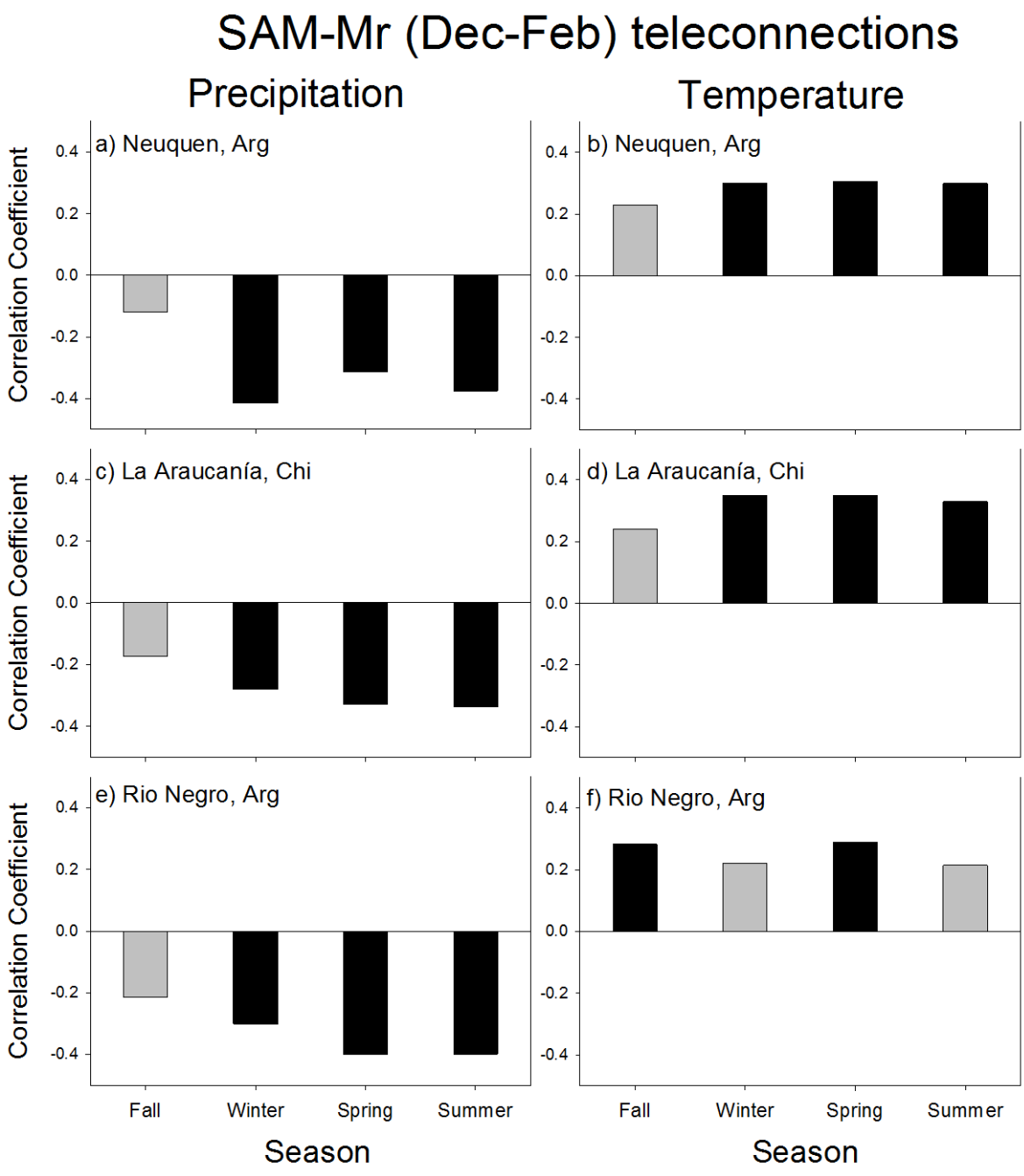
SAM-Mr (Dec-Feb) teleconnections
Precipitation
Temperature
a) Neuquen, Arg
b) Neuquen, Arg
c) La Araucanía, Chi
d) La Araucanía, Chi
e) Rio Negro, Arg
f) Rio Negro, Arg
Correlation Coefficient
0.4
0.2
0.0
-0.2
-0.4
Fall
Winter
Spring
Summer
Season

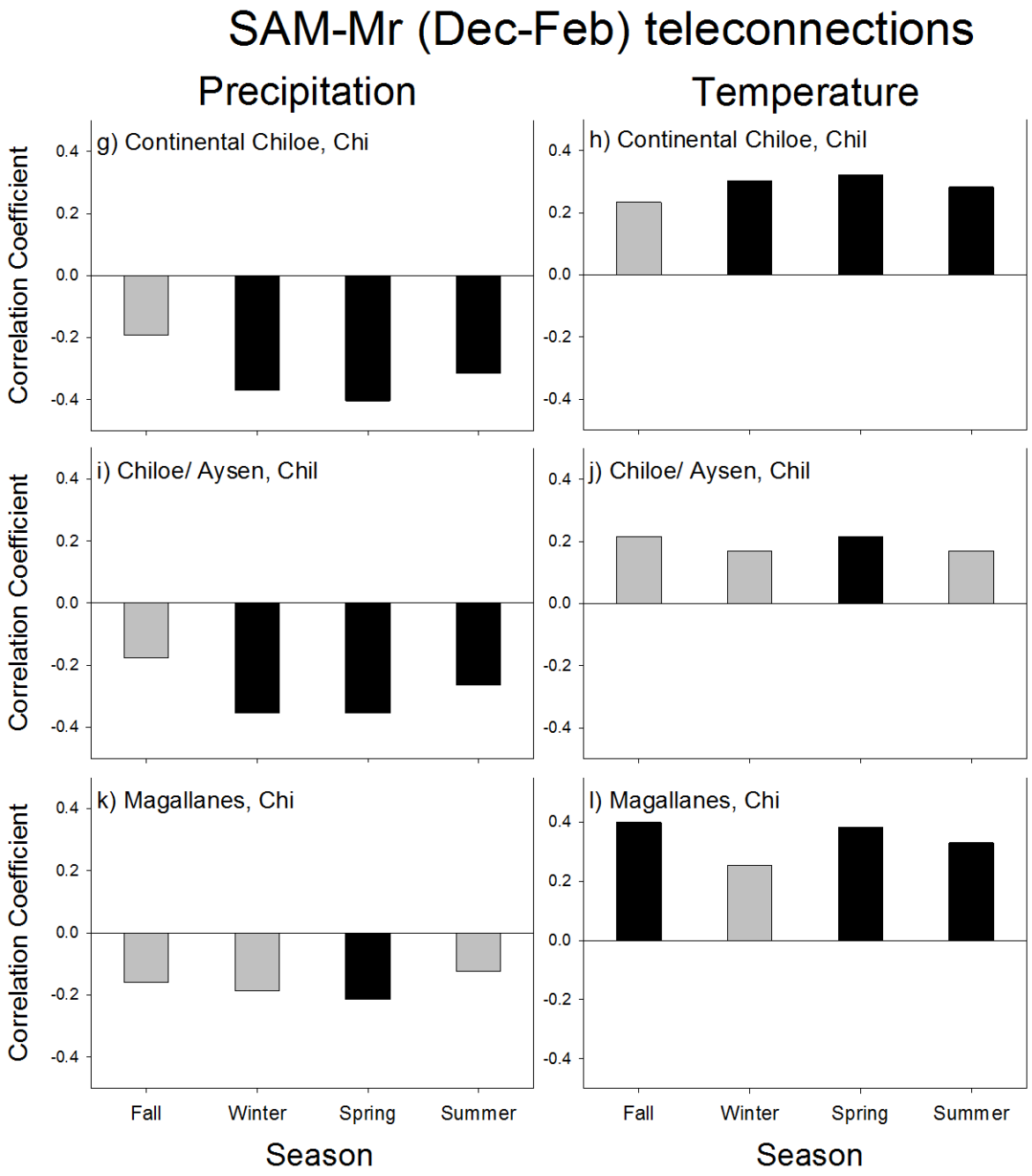

Figure S4. Correlation functions relating variability in seasonal (Fall: MAM, Winter: JJA, Spring: SON, and Summer: DJF) precipitation and temperatures from gridded climate records (0.5x0.5; CRU TS3.22) representing each study area to the summer SAM index (DJF; Marshall; 1957-2013). Bootstrapped confidence intervals were computed to estimate statistical significance of correlation function coefficients.

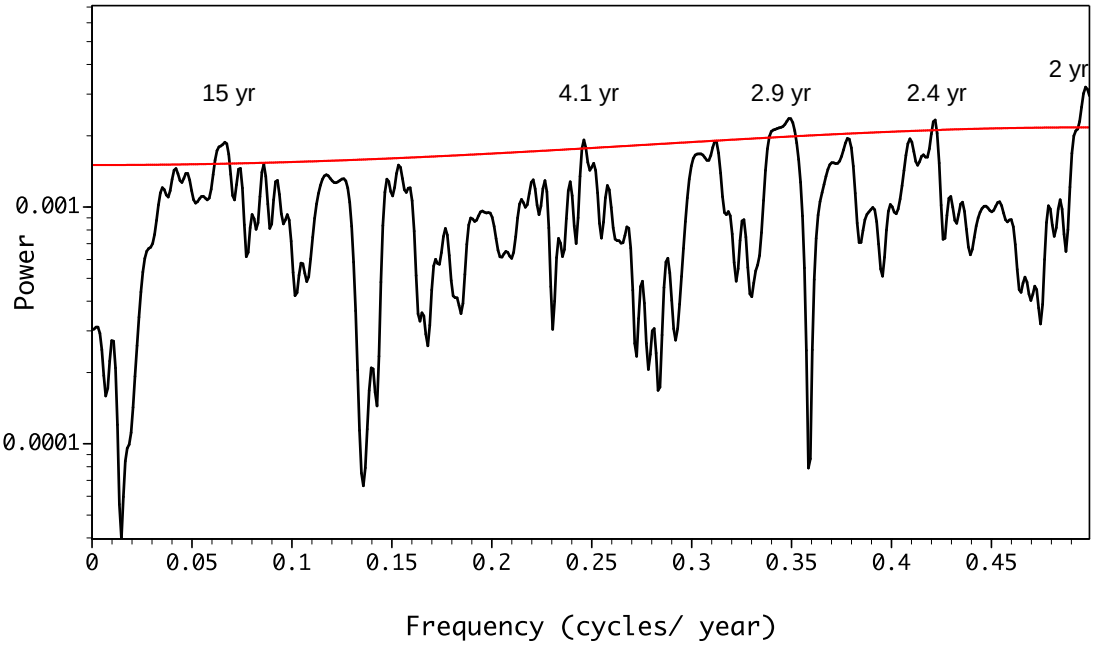

Fig. S5. Power spectra of the index of Sub-Continental Fire Activity (SCFA, with changing sample depth) using the MultiTaper method (MTM) for the 1738-1932 period; the record starts with a minimum of 10% of recording sites and ends when fire suppression began. Red line indicates AR(1) CI= 90%.

ST1: Supplementary Text.

Caveats and limitations

Changes in the patterns of human ignitions were not quantitatively assessed in the current study because tree-ring and charcoal evidence of past fire cannot conclusively determine ignition sources. Data on lightning versus human sources of ignition are only available in the documentary fire record for the Argentine sites after c. 1942 and for the Chilean sites after c. 2000. Previous studies have inferred the impact of humans on fire activity from correlations of fire with known human population changes and comparison of areas of differing levels of human occupation in nearby and similar habitats (i.e. from Indigenous to modern settlers, to fire suppression (5, 8, 7, 9). Climate-caused spikes in fire activity are commonly identified as synchronous patterns over large spatial extent in disjunct areas that reflect control by the regional climate. In the current study only in a limited area (Neuquén), clear effects of a fire suppression policy starting in the 1930s were exhibited. The sub-continental indices of fire synchrony and activity patterns found in this study indicate years of widespread fire that could only be explained by broad-scale climate variability, not by synchronous changes in frequencies of human-set fires or fire suppression.

Two regions (NW Argentina and Central Chile) for which tree-ring fire-scar histories are available had records of widespread fire (i.e. years of ≥ 2 fire-scarred trees per site with a minimum of four trees capable of recording fire per site at 10% or more sites per region) that only began in the mid-20th century, and consequently these two northernmost regions

(i.e. north of 37°S) were not included in any of the regional nor sub-continental scale analyses. Instead, regional and sub-continental scale analyses were reported using the remaining six regions located south of 37°S.

Precipitation reconstructions

A single time series (Fig. 3a in (15)) was used in our climate-fire analyses (i.e. Fig. 2d) at sub-continental scales because a) this single reconstruction shows relatively little spatial variability in after 1700AD for the area south of c. 35°S, b) this reconstruction was designed to be used as a single time series (i.e. avoid the use of sub-regions; Neukom, R. *pers. comm*.), and c) the geographic extent of our sub-continental fire indices matches well the SSA-scale of this precipitation reconstruction.

Delayed wavelet coherence analyses

Delayed coherence between the climate and fire indices over the analyzed 1738-1932 period is indicated when arrows are neither in-phase (right) nor anti-phase (left). For example, when arrows are pointing straight down (90°; $\pi/2$), fire indices are delayed or lagged from the climate indices by a ¼ cycle at a particular frequency or coherence period. In the case when arrows are pointing straight up, fire indices can be either delayed by 90° from the climate indices by a ¼ cycle at a particular frequency or anti-phase coherence period or by 270° from the climate indices by a ¾ cycle at a particular frequency or phase coherence period (16, 17).

Supplementary Information References

1. Aráoz E & Grau HR (2010) Fire-Mediated Forest Encroachment in Response to Climatic and Land-Use Change in Subtropical Andean Treelines. *Ecosystems* 13(7):992-1005.
2. Grau HR & Veblen TT (2000) Rainfall variability, fire and vegetation dynamics in neotropical montane ecosystems in north-western Argentina. *Journal of Biogeography* 27(5):1107-1121.
3. Gómez-González S*, et al.* (2011) Anthropogenic fires increase alien and native annual species in the Chilean coastal matorral. *Diversity and Distributions* 17(1):58-67.
4. Mundo IA, Kitzberger T, Roig Juñent FA, Villalba R, & Barrera MD (2013) Fire history in the Araucaria araucana forests of Argentina: human and climate influences. *International Journal of Wildland Fire* 22(2):194-206.
5. Veblen TT, Kitzberger T, Villalba R, & Donnegan J (1999) Fire history in northern Patagonia: The roles of humans and climatic variation. *Ecological Monographs* 69(1):47-67.
6. Quezada JM (2008) Historia de incendios en bosques de Araucaria araucana (Mol.) Koch del Parque Nacional Villarrica, a partir de anillos de crecimiento y registros orales. P.E. Forest Engineering (University Austral, Valdivia, Chile).
7. González ME, Veblen TT, & Sibold JS (2005) Fire history of Araucaria-Nothofagus forests in Villarrica National Park, Chile. *Journal of Biogeography* 32(7):1187-1202.
8. Holz A & Veblen TT (2011) The amplifying effects of humans on fire regimes in temperate rainforests in western Patagonia. *Palaeogeography, Palaeoclimatology, Palaeoecology* 311(1-2):82-92.
9. Kitzberger T & Veblen TT (1997) Influences of humans and ENSO on fire history of Austrocedrus chilensis woodlands in northern Patagonia, Argentina. *Ecoscience* 4(4):508-520.
10. Holz A, Kitzberger T, Veblen TT, & Paritsis J (2012) Ecological and climatic controls of modern wildfire activity patterns across southwestern South America. *Ecosphere* 3(11):103.
11. González ME & Veblen TT (2006) Climatic influences on fire in Araucaria araucana-Nothofagus forests in the Andean cordillera of south-central Chile. *Ecoscience* 13(3):342-350.
12. Holz A, Haberle S, Veblen TT, De Pol-Holz R, & Southon J (2012) Fire history in western Patagonia from paired tree-ring fire-scar and charcoal records. *Climate of the Past* 8:451-466.
13. Holz A & Veblen TT (2012) Wildfire activity in rainforests in western Patagonia linked to the Southern Annular Mode. *International Journal of Wildland Fire* 21(2):114-126.
14. Villalba R*, et al.* (2012) Unusual southern Hemisphere tree growth patterns induced by changes in the Southern Annular Mode. *Nature Geoscience* 5:793–798.
15. Neukom R*, et al.* (2010) Multi-centennial summer and winter precipitation variability in southern South America. *Geophysical Research Letters* 37.
16. Torrence C & Webster PJ (1999) Interdecadal Changes in the ENSO–Monsoon System. *Journal of Climate* 12(8):2679-2690.
17. Grinsted A, Moore JC, & Jevrejeva S (2004) Application of the cross wavelet transform and wavelet coherence to geophysical time series. *Nonlin. Processes Geophys.* 11(5/6):561-566.